metals

MDPI

Article

Interaction of Process Parameters, Forming Mechanisms, and Residual Stresses in Single Point Incremental Forming

Fabian Maaß *, Marlon Hahn and A. Erman Tekkaya

Institute of Forming Technology and Lightweight Components, TU Dortmund University, Baroper Str. 303, 44227 Dortmund, Germany; marlon.hahn@iul.tu-dortmund.de (M.H.); erman.tekkaya@iul.tu-dortmund.de (A.E.T.)

* Correspondence: fabian.maass@iul.tu-dortmund.de; Tel.: +49-231-755-2607

Received: 23 March 2020; Accepted: 15 May 2020; Published: 19 May 2020

Abstract: The residual stress state of a sheet metal component manufactured by metal forming has a significant influence on the mechanical properties, and thus determines the time until the component fails, especially for dynamic loads. The origin of the resulting residual stress state of incrementally formed parts with regard to the forming mechanisms of shearing, bending, and the normal stress component is still under investigation. The relationship between the process parameters, the forming mechanisms, and the resulting residual stress state for a complex part geometry manufactured by single point incremental forming (SPIF) is presented in this publication. For this purpose, a validated numerical process model is used to analyze the influence of the step-down increment Δz for truncated cones on the characteristics of the forming mechanisms and the resulting residual stress state. For the first time the forming mechanisms are evaluated numerically on both sides of the formed component. A relationship between the process parameters, forming mechanisms, residual stresses, and the mechanical properties of an incrementally formed component is shown. Shearing-induced hardening is identified as a relevant influence on the residual stress state of cones.

Keywords: single point incremental forming; forming mechanisms; residual stress state

1. Introduction

The high formability in incremental sheet metal forming is a result of stress superposition during the process in a locally confined area that reduces the process forces and enables the processing of high-strength materials and complexly shaped components in a single setup compared to conventional forming processes. The complex relation of stress formation during the forming process that leads to the increased formability is due to the superposition of the forming mechanisms bending, shearing, and normal components [1]. The appearance of the forming mechanisms is described in various publications. The influence of each forming mechanism on the forming process has been discussed in different ways and is still not clear. Silva et al. [2] indicate the influence of membrane stretching as an important mechanism in single point incremental forming (SPIF) related to the sheet thickness reduction. Sebastiani et al. [3] experimentally demonstrated membrane stretching perpendicular to the tool movement direction. This effect increases by decreased vertical tool step-down increments and forming tool diameters [4]. The influence of the bending mechanism as an essential forming mechanism is proposed by Emmens et al. [1]. Larger strains on the tool side than on the tool-averted side and non-linear stresses on the tool side are shown as results of the bending mechanism during the forming operation [5]. In SPIF, bending always occurs in combination with a stretching component perpendicular to the tool feed [6], therefore additional tensile residual stresses on the tool side can

be measured. Sebastiani et al. [3] detected larger plastic strains perpendicular to the tool feed on the tool side than on the tool-averted side. Recently, Maqbool et al. [4] explained the poor geometry accuracy as a result of bending-related springback effects. The importance of the shearing mechanism for this process is related to the comparison of single point incremental forming and the process of metal spinning [7,8]. Three different types of shearing that are relevant for SPIF can be distinguished. In-plane shear [9,10], shearing through the sheet thickness, and out-of-plane shear [3]. Maqbool et al. [4] demonstrated increasing through-thickness shear in the tool direction with decreasing step-down increment, increasing sheet thickness, or increased friction. Additionally, through-thickness shear increases with higher wall angles [11]. The shear due to the tool feed leads to a shear gradient in through-thickness direction [12], but is not an essential forming mechanism for incremental sheet metal forming [3]. Silva et al. [2] explained by membrane theory that stretching, not shear, is the dominant forming mechanism in the SPIF process. Out of plane shear was only proposed by numerical investigations and not yet validated [8]. The contact pressure of the forming tool during the forming operation leads to additional compressive stresses in the forming zone. These compressive stresses stabilize the forming process and lead to an increased formability by increasing the flow stress of the material [13]. In a recent publication [14], the influence of the forming mechanism on the residual stress development for simple linear groove geometries was analyzed. The influence of the step-down increment was shown by texture analysis.

In this work, the dependence of the forming mechanisms shearing, bending, and normal components on the process parameter $\Delta z/R_{\mathrm{Tool}}$ is shown by forming a complex component geometry. The step-down increment Δz is varied in a numerical process model while the tool radius R_{Tool} and the other process parameters as well as the final geometry are kept constant. The numerical process model is validated by comparing the vertical tool force, the component geometry, and the sheet thickness with experiments. The determination of the resulting residual stresses and their development with regard to the forming mechanisms, as a result of the process parameter adjustment, is then carried out numerically. It is shown how the residual stress state is influenced by the forming mechanisms. Based on published results linking the relationship between the residual stress state and the fatigue strength of a component, it is shown how the forming mechanisms affect the mechanical properties of the manufactured components.

2. Materials and Methods

For the validation of the numerical process model truncated cone geometries are manufactured by single point incremental forming. The dimensions of the truncated cone geometry are shown in Figure 1a. A conventional 5-axis DMU 50 milling machine from DMG Mori (Bielefeld, Germany) was used for this step (Figure 2a). The truncated cones were made of aluminum alloy AA5083 with an initial sheet thickness of t_0 = 1 mm. The production is carried out with a bidirectional tool path with a driven forming tool with a spherical end and a radius R_{Tool} = 7.5 mm (Figure 1b). The step-down increment is varied in three steps: Δz_{24} = 1.875 mm, Δz_{12} = 3.75 mm, and Δz_{8} = 5.625 mm. All other process parameters are kept constant according to Table 1. The sheet was fixed with a clamping frame (Figure 2b). A deep-drawing oil (Castrol Iloform PN 226) was applied to the sheet metal surface as lubrication.

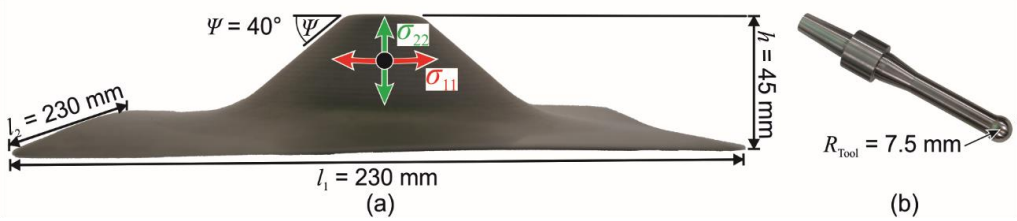

Figure 1. (**a**) Dimensions of truncated cone geometry and evaluation point; (**b**) Forming tool.

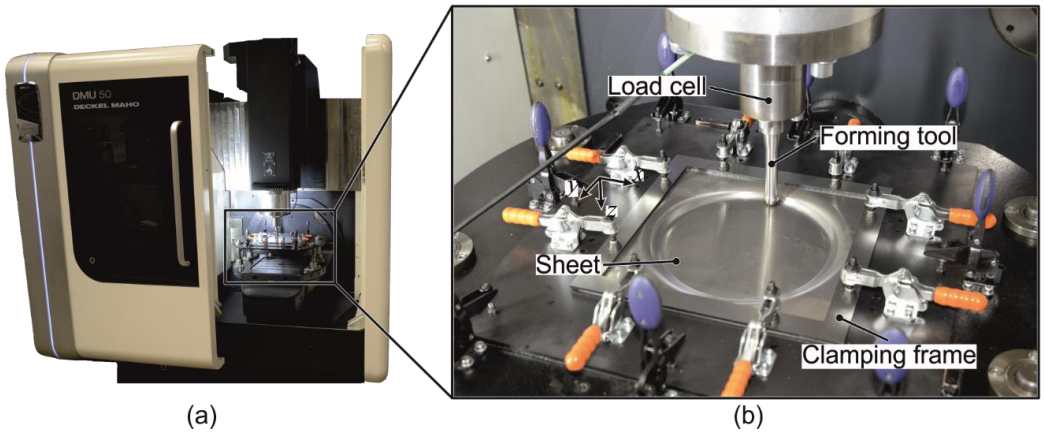

Figure 2. Experimental process setup: (**a**) 5-axis milling machine with (**b**) single point incremental forming experimental setup.

The process force of the force component F_z was determined using a 3-component piezoelectric force sensor (Figure 2b). Only the force component in the z-direction is considered here. To determine the geometrical deviation and the distribution of sheet thickness, a three-dimensional measurement is performed using the optical digitizer ATOS Triple Scan form GOM (Braunschweig, Germany). A precise fringe pattern is projected onto the surface of the object and recorded by two cameras. Based on the stereo camera principle, a 3D model of the part is generated. The sheet thickness distribution of the formed component can be determined locally using a scan of the front and back side of the part. Since the residual stress state of a component is highly dependent on the geometry, it must be ensured that a variation of the process parameters and a resulting change of the residual stress is not due to a deviation of the final geometry.

Table 1. Process parameters.

Process Parameters	8 Increments	12 Increments	24 Increments
Tool radius R_{Tool}	7.5 mm	7.5 mm	7.5 mm
Step-down increment Δz	5.625 mm	3.75 mm	1.875 mm
Relative tool step-down $\Delta z/R_{\mathrm{Tool}}$	0.75	0.5	0.25
Tool feed v_{Tool}	1500 mm/min	1500 mm/min	1500 mm/min
Tool rotation θ_{Tool}	300 RPM	300 RPM	300 RPM

The numerical model of the process was built in ABAQUS/Explicit and consists of the forming tool as a rigid body and the elastic-plastic sheet metal built of solid elements (C3D8) with an edge length of 1 mm and five elements over the sheet thickness (Figure 3). An explicit time integration with a time step of 1×10^{-06} was used. The computations are done using the high performance cluster (HPC) LiDO3. The total CPU time spent was approximately 32 h.

Figure 3. Numerical process model setup.

The material model for the sheet includes combined isotropic-kinematic hardening based on Chaboche. The AA5083 base material was characterized using the uniaxial tensile test and in-plane torsion test (Figure 4) according to Maaß et al. [14]. The material coefficients in Table 2 are determined inversely using the cyclic loading test results according to Chaboche's procedure [15]. The initial flow stress of the material was determined to be $\sigma_{f,0}$ = 165 MPa. A penalty contact is used for forming tool and sheet. The friction coefficient between the well lubricated forming tool and the sheet was set to μ = 0.03 as revealed in strip-tension tests. The numerical simulation starts with a simulation of the incremental single point forming process with ABAQUS/Explicit including mass scaling (mass scaling factor 10^3). The explicit simulation to evaluate the forming mechanisms is followed by a subsequent implicit simulation of the unclamping to determine the residual stresses.

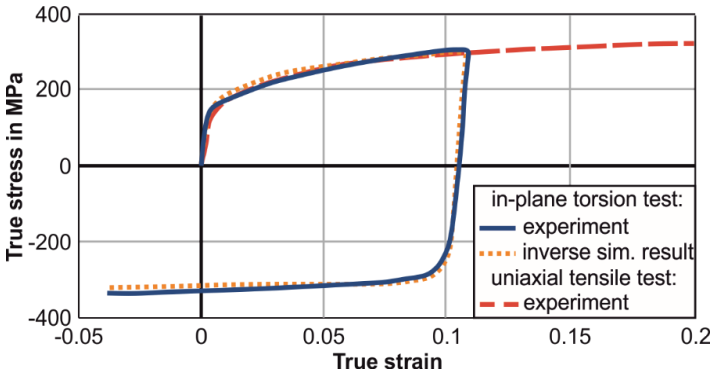

Figure 4. Material characterization of aluminum alloy 5083.

Table 2. Characteristic Chaboche coefficients of AA 5083.

Young's Modulus E	Poisson's Ratio υ	k	Q	b	C	γ
73,000 MPa	0.33	120 MPa	83 MPa	9.88	30,000	330

3. Results

The process force, the geometry, and sheet thickness distribution from the experiments are used for the validation of the numerical model.

3.1. Process Force

A comparison of the experimentally measured in-situ process forces F_z for the three different step-down increments Δz is shown in Figure 5.

An increasing step-down increment Δz results in a reduction in the process time. The maximum process force F_z of the considered process window corresponds to a reduction of 46% comparing 24 increments ($F_{z,24}$ = 1.89 ± 0.04 kN) and 8 increments ($F_{z,8}$ = 3.49 ± 0.07 kN). There is good agreement between the experimental and the numerical results with a maximum deviation of 8%. The peak forces are a result of the tool step-down. The time span between two peaks decreases due to the decreasing diameter of the tool path circle with increasing depth of the cone.

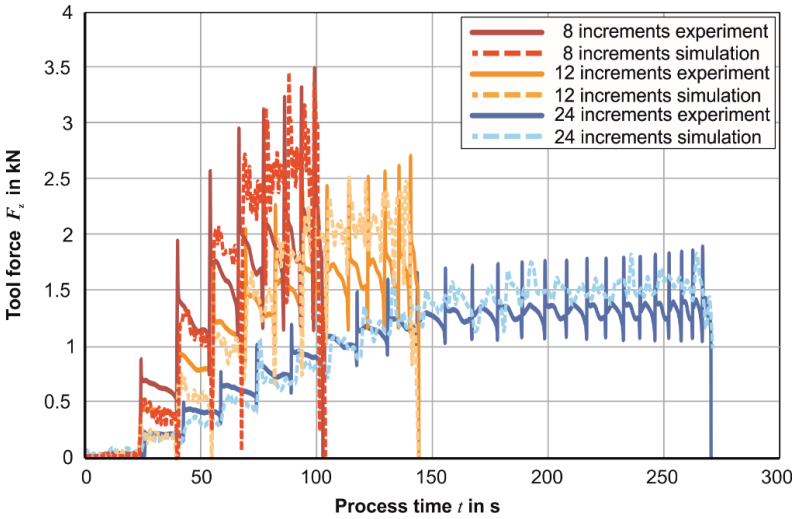

Figure 5. Experimentally and numerically determined process forces for 8 increments, 12 increments, and 24 increments of the same final geometry.

3.2. Geometry

A comparison of the geometry (cut A-A) of experimental results is shown in Figure 6a. With a decreasing number of step-down increments, there is an increasing waviness of the inner surface due to the increase of the step-down increment amount (Figure 6b). The maximum geometric deviation from the CAD target geometry is 11% due to process-related springback effects. The deviation is defined as the maximum distance between two points on the profiles with the same x-coordinate. The highest deviation is measured in the flange area after unclamping. However, the accuracy of the final geometry increases with a decreasing number of step-down increments due to an increased springback as shown in Ambrogio et al. [16], the maximum deviation between the three final geometries is 4.8%. Therefore, it can be assumed that a variation of the step-down increment, within the examined limits, has no significant effect on the resulting geometry of the component.

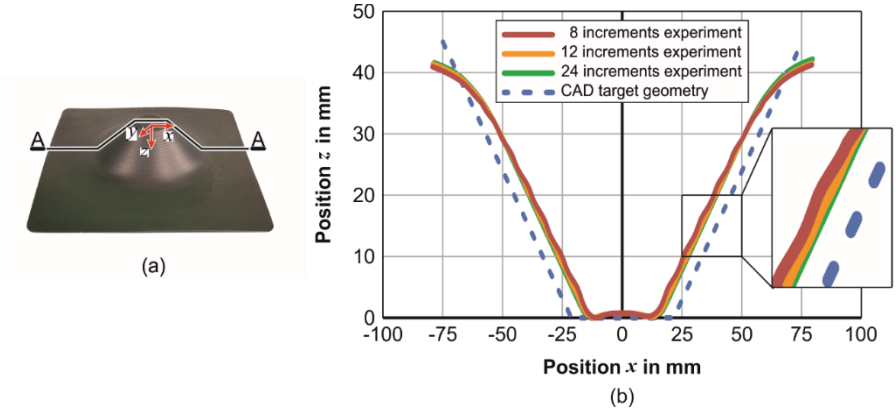

Figure 6. (**a**) Cut A-A position; (**b**) Experimental geometry (cut A-A) and target geometry profile.

Regarding the numerical results, a comparison of the final experimental geometry and the numerically determined geometry of the truncated cone is shown in Figure 7.

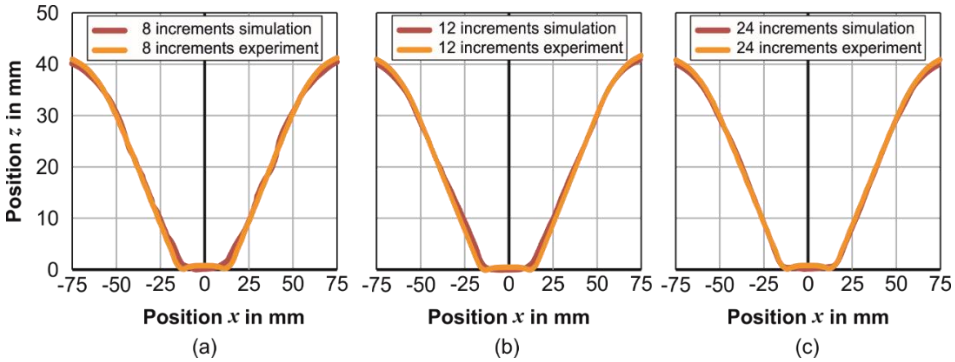

Figure 7. Comparison of numerical and experimental geometry (cut A-A): (**a**) 8 increments; (**b**) 12 increments; (**c**) 24 increments.

An increasing number of increments leads to an improved geometrical accuracy. The maximum deviation improves $\Delta z_{max,8} = 0.67 \pm 0.01$ mm for eight increments to just $\Delta z_{max,24} = 0.49 \pm 0.01$ mm for 24 increments used.

3.3. Sheet Thickness

The sheet thickness distribution along the cut A-A is shown in Figure 8. The initial sheet thickness of $t_0 = 0.96 \pm 0.01$ mm decreases with an increasing number of step-down increments. The decreasing sheet thickness reduction varies between 26.8% for 8 increments (Figure 8a) and 44.7% for 24 increments (Figure 8c). The experimentally determined sheet thickness is smoothened to reduce the high level of noise due to the light reflections during the optical sheet thickness measurement. The maximum deviation between experiment and numerical results is 9% for the sheet thickness. With a decreasing number of increments, the thickness distribution along the cone wall gets more homogeneous. Depending on the incremental depth Δz some part of the material is deformed repeatedly due to an overlap when the forming tool is moving forward along the tool trajectory. If the number of increments is decreased there are less over-laps [17]. Due to the incremental forming of the cone wall, the initial sheet thickness is only reduced in the cone wall area. In the clamped flange area and the unformed bottom area of the part, the initial sheet thickness remains constant.

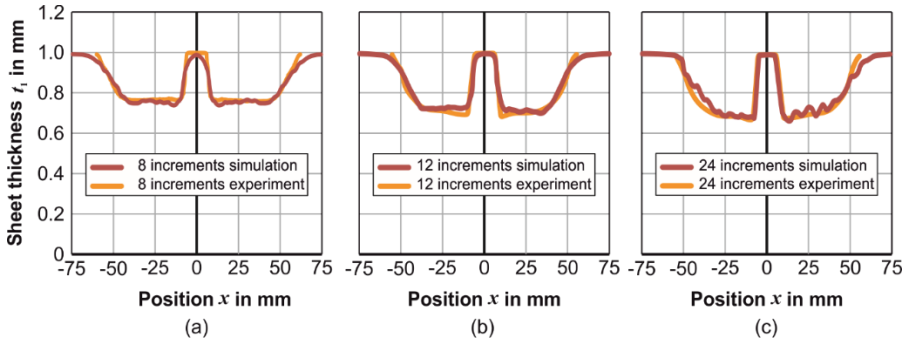

Figure 8. Comparison of numerical and experimental sheet thickness distribution (cut A-A): (**a**) 8 increments; (**b**) 12 increments; (**c**) 24 increments.

3.4. Hardness

Vickers hardness measurements enable the identification of various mechanical properties. The Vickers hardness measurement corresponding to HV 5.0 is used to determine the average hardness of the initial sheet (Figure 9a).

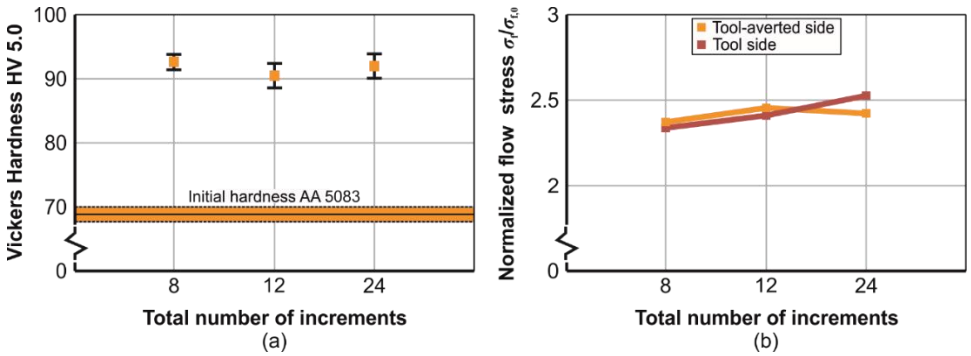

Figure 9. (**a**) Experimental hardness measurements; (**b**) Numerically evaluated normalized flow stress.

The measurements are carried out using the cross-sections of the component opposite to the step-down mark in the middle of the formed cone wall with three repetitions considering the whole sheet thickness. The initial material hardness of the AA 5083 base material of 68.9 HV 5.0 is significantly increased by the process.

Regarding the number of increments, the strain-induced hardening is stationary with an increasing number of increments (Figure 9a). Figure 9b presents the normalized flow stress $\sigma_f/\sigma_{f,0}$ at the tool-side and the tool-averted side for a different number of increments. The normalized flow stress is increased with an increasing number of increments while the experimental hardness measurements are stationary (Figure 9a). The increase on the tool-averted side is higher than on the tool side for the amount of increments, but there is a turnover with an increasing number of increments.

3.5. Residual Stresses

The residual stress prediction of the numerical model was already experimentally validated by residual stress measurements using X-ray diffraction in Maaß et al. [14]. In this publication residual stresses were measured on both sides of linear grooves in tool feed direction and perpendicular to the tool path direction in the same measuring point. The overall variation of the numerical results compared to the experimental results was determined as 7%. For the present study, the residual stress amplitudes are output on both sides of the sheet in the center of the formed component wall at a height of 22.5 mm (middle of the cone wall, Figure 1a). The stress distribution of σ_{22} residual stresses in the cone wall is almost rotationally symmetric (except for the tool step-down area) and follows the pattern shown as an example for a sliced area around the evaluation point in Figure 10.

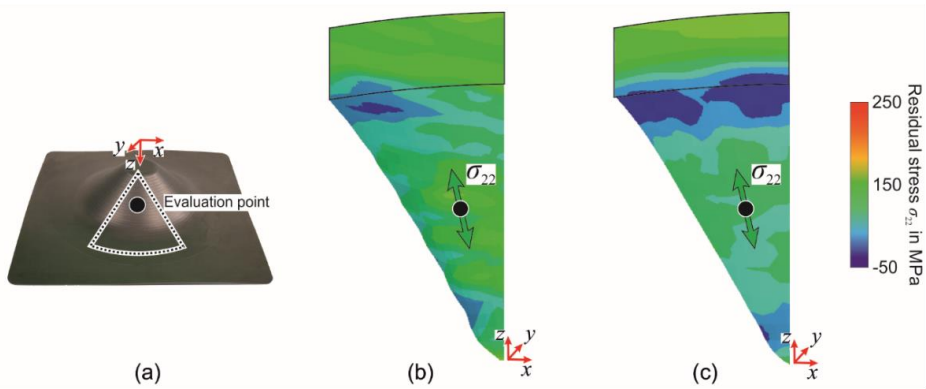

Figure 10. Residual stresses distribution of σ_{22}-component in the cone wall slice around the evaluation point (**a**) at the tool side for: (**b**) 8 increments and (**c**) 24 increments.

The residual stress in the evaluation point are output nearest to the surface along through thickness direction at the tool side and the tool averted. The local stress components in tangential direction σ_{11}

and meridional direction σ_{22} to the cone wall surface for the tool side and tool-averted side are shown in Figure 11.

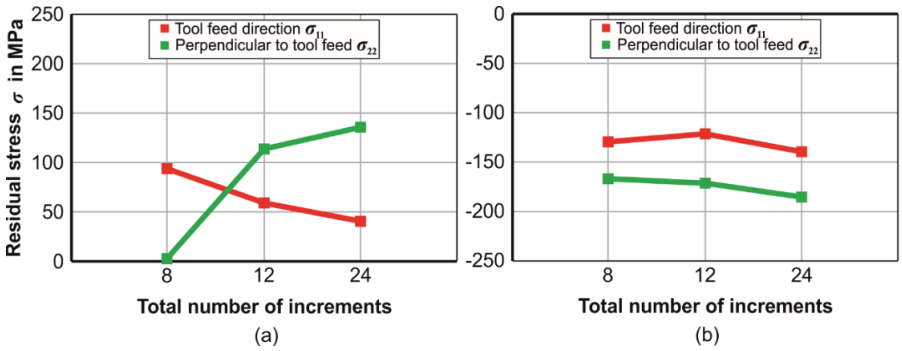

Figure 11. Residual stresses evaluated in the middle of the formed cone wall at an integration point on the surface of: (**a**) tool side and (**b**) tool-averted side.

Considering the residual stresses σ_{22}, that are perpendicular to the tool feed direction during one cycle transverse to the plane, the tensile residual stresses on the tool side increase monotonously from zero up to $\sigma_{22} = 144$ MPa when increasing the number of increments. The change of the residual stresses on the tool-averted side is less distinct with an increasing number of increments. The residual stresses rise to $\sigma_{22} = -179$ MPa for 24 increments from $\sigma_{22} = -161$ MPa for eight increments. In an opposing trend on the tool side, residual stresses in the tool feed direction σ_{11} decrease with an increasing number of increments. The tensile residual stresses in the tool feed direction σ_{11} on the tool-averted side follow those of the tool feed direction σ_{22} on the tool-averted side and are rather stationary. The residual shear stress component σ_{12} remains almost stationary with an increasing number of increments in the range of the σ_{11} component for 24 increments on the tool side. On the tool averted-side, σ_{12} also remain stationary in the range of $\sigma_{12} = -20$ MPa.

3.6. Forming Mechanisms

The forming mechanisms are quantified as described in Maaß et al. [18]. Derived from the output of the stress and strain components of the numerical model, the forming mechanisms are evaluated at the point of interest depicted in Figure 1a according to the locally defined 1-, 2- and 3-directions. The integration points of five linear brick elements in through thickness direction with four integration points in two planes per element are evaluated regarding the relevant stress and strain components σ_{ij} (Cauchy stress) and $d\varepsilon_{ij}$ (total logarithmic strain increment). The normal stress components of a volume element, which represent the tension compression part, are named σ_{n1}, σ_{n2}, σ_{n3}, and are the average values of, e.g., σ_{11} over all volume elements through the sheet thickness. This gives four values of e.g., σ_{n1} per element. The shearing components σ_{12}, σ_{23}, σ_{13} are the direct tensor output values of ABAQUS at a considered integration point (1). The incremental strain components are treated equally (2).

$$\sigma_{ij} = \begin{pmatrix} \sigma_{11} & \sigma_{12} & \sigma_{13} \\ \sigma_{21} & \sigma_{22} & \sigma_{23} \\ \sigma_{31} & \sigma_{32} & \sigma_{33} \end{pmatrix} \quad (1)$$

$$d\varepsilon_{ij} = \begin{pmatrix} d\varepsilon_{11} & d\varepsilon_{12} & d\varepsilon_{13} \\ d\varepsilon_{21} & d\varepsilon_{22} & d\varepsilon_{23} \\ d\varepsilon_{31} & d\varepsilon_{32} & d\varepsilon_{33} \end{pmatrix} \quad (2)$$

As an assumption, pure bending components in terms of both stress and strain cancel out when integrating over the sheet thickness giving the normal components mentioned above. Only the bending components around the 1- and 2-directions are considered. Bending around the 3-direction is not

present in the SPIF process and is therefore neglected. The components for bending (index b) are then defined by the superposition according to Equations (3) and (4).

$$\sigma_{bi} = \sigma_{ii} - \sigma_{ni}\,, i = 1,\ 2 \tag{3}$$

$$d\varepsilon_{bi} = d\varepsilon_{ii} - d\varepsilon_{ni}\,,\quad i = 1,\ 2 \tag{4}$$

The determination of the specific dissipated energy is then done by evaluating each forming mechanism for the considered volume element according to Equations (5)–(7) where the integration limits are from $t = 0$ until the process end. It is noted that these values are the average values of all integration points of an element.

$$w_{\text{Normal}} = \int \sigma_{n1} d\varepsilon_{n1} + \int \sigma_{n2} d\varepsilon_{n2} + \int \sigma_{33} d\varepsilon_{33} \tag{5}$$

$$w_{\text{Shearing}} = \int \sigma_{12} d\varepsilon_{12} + \int \sigma_{23} d\varepsilon_{23} + \int \sigma_{13} d\varepsilon_{13} \tag{6}$$

$$w_{\text{Bending}} = \int \sigma_{b1} d\varepsilon_{b1} + \int \sigma_{b2} d\varepsilon_{b2} \tag{7}$$

The resulting values are verified by comparing the sum of all energy values with the total plastic internal energy dissipation given by ABAQUS, $w_{tot} = w_{\text{Normal}} + w_{\text{Shearing}} + w_{\text{Bending}}$. The forming mechanisms are calculated at the near-surface elements at the tool side and at the opposite tool-averted side.

An evaluation of the forming mechanisms on the tool side shows a significant and continuous increase of shear with an increasing number of step-down increments (Figure 12a).

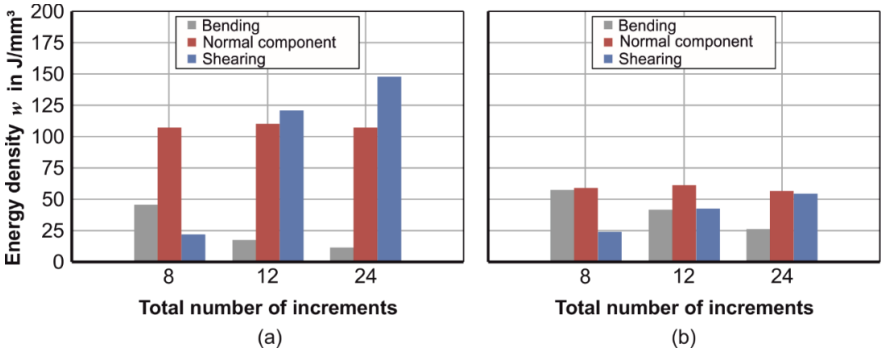

Figure 12. Elemental energy density evaluated in the middle of the formed cone wall: (**a**) tool side; (**b**) tool-averted side.

Simultaneously, the bending mechanism decreases continuously with an increasing number of increments, in an opposing trend. The normal component on the tool side varies within a small range, remaining almost constant with an increasing number of step-down increments. At the tool-averted side, the qualitative development of the forming mechanisms is equal to the tool side (Figure 12b). However, the forming mechanisms shearing and the normal components are at a lower level than on the tool side. The bending mechanism is slightly higher on the tool-averted side than on the tool side. Although the used element type may be prone to shear locking, this was not an obvious problem in the presented study as both the displacements or geometry and the forces were validated experimentally, meaning that a stiffness over prediction was not observed in the simulation results.

4. Discussion

The accordance of the geometry profiles within the examined number of step-down increments (Figure 6b) suggests that a change in the residual stress state with regard to the number of increments used from $\sigma_{22.8}$ = 5 MPa to $\sigma_{22.24}$ = 140 MPa on the tool side (Figure 11) is not primarily caused by a change in geometry. It can be seen that the increase in residual stress amplitudes is due to the process-related decrease in sheet thickness (Figure 8) and the associated material hardening of the initial AA5083 base material (Figure 9a). The reasons for these effects are identified evaluating the acting forming mechanisms shearing, bending, and the normal components (Figure 12). In particular, the shearing, which increases solely with an increasing number of increments, seems to have an influence on the decrease in sheet thickness and the hardening of the material during the process. An increasing number of step-down increments strengthens shearing due to the high portion of already plasticized and hardened areas in the forming zone. The normal component, which reaches a higher level on the tool side due to the forming tool pressure, shows no significant dependence on the number of increments. The fact that σ_{22} is the only residual stress that increases in the tensile range on the tool side (Figure 11a) could, thus, be explained by the increasing amount of shearing when the number of increments is increased (Figure 12a) since no other mechanism increases. This increase in shearing, which can be observed on both sides of the sheet, therefore causes the strain hardening (Figure 9). The hardening-induced increasing normalized flow stress (Figure 9b) enables the material to take a higher absolute amount of residual stress amplitudes [19]. Due to the kinematic process of the SPIF process, residual stresses are more pronounced on the tool side than on the tool-averted side.

On the tool-averted side, the amplitudes of the compressive residual stresses are stationary with an increasing number of increments. Analyzing the forming mechanisms shows an increase in shearing and a decrease in bending as well as a stationary behavior of the normal component on the tool-averted side with an increasing number of step-down increments (Figure 12b). Due to the lower level of shearing compared to the tool side (Figure 12a), the bending gains a relative influence. Although the experimentally determined hardness measurements show a notable increase in material hardness compared to the initial state, the different effects on the tool and tool-averted sides are blurred due to the large test indention of HV 5.0. A clear distinction between tool and tool-averted side is not possible.

Regarding the effects of residual stresses on the mechanical properties, Maaß et al. [20] provide detailed information. Using a cyclic loading test setup of heat-treated and not heat-treated specimens, as explained in Maaß et al. [20], with an increasing number of increments, the relationship between residual stresses on the tool side and the failure of a component is shown (Figure 13). The failure can be clearly assigned to the residual stresses by comparing stressed specimens and stress-relieved specimens. A relationship between the tensile residual stresses on the tool side and a 42% reduction of the lifetime in cyclic load tests until a component failure is experimentally shown.

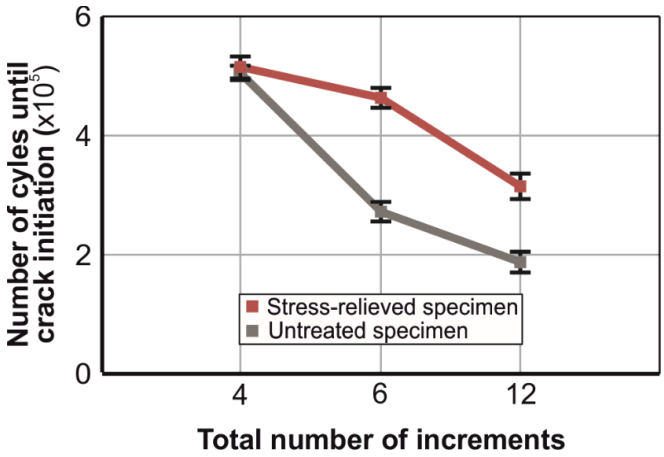

Figure 13. Cyclic loading test [20].

5. Conclusions and Outlook

It can be concluded that there is a direct relation between the process parameter step-down increment, the forming mechanisms, and the resulting residual stress state, which significantly influences the component properties. The component properties can be optimized for a specific load case by a targeted induction of the residual stresses in the component. According to the load case of the formed component, the product properties can be directly influenced by adjusting the residual stress state. A basic understanding of the relationship between the process parameters and the residual stress formation in the process is necessary for the targeted setting of the residual stress state according to the application. This publication explains the influence of the process parameter relative step-down increment $\Delta z/R_{\mathrm{Tool}}$ on the forming mechanisms of the incremental sheet metal forming process and the resulting residual stress state in the component by a validated numerical process model. Due to the increasingly dominant shearing mechanism with an increasing number of step-down increments, the material thickness is reduced and hardened, particularly on the tool side. Beside other effects, the material hardening enables a higher residual stress amplitude in the material, the leads to higher residual stress amplitudes. As a result, the increased initial tensile residual stresses on the tool side lead to an early failure of a truncated cone under cyclic loading.

Further investigations should focus on the examination of the transferability of results to materials with significantly different hardening behavior compared to the analyzed material AA5083. A suitable experimental validation of the forming mechanisms could be carried out to confirm the numerically determined portions of the forming mechanisms.

Author Contributions: Conceptualization, F.M., A.E.T.; methodology, F.M.; validation, F.M.; investigation, F.M.; writing—original draft preparation, F.M.; writing—review and editing, F.M., M.H., A.E.T.; supervision, A.E.T.; project administration, F.M. and A.E.T.; funding acquisition, F.M., M.H., A.E.T. All authors have read and agreed to the published version of the manuscript.

Funding: Funded by the German Research Foundation (DFG, Deutsche Forschungsgemeinschaft).

Acknowledgments: The authors would like to thank the German Research Foundation (DFG, Deutsche Forschungsgemeinschaft) for funding the research project 372803376 as part of the priority programme SPP 2013 "The utilization of residual stresses induced by metal forming". We acknowledge the financial support by the German Research Foundation and TU Dortmund University within the funding programme Open Access Publishing.

Conflicts of Interest: The authors declare no conflict of interest.

References

1. Emmens, W.; van den Boogaard, A. An overview of stabilizing deformation mechanisms in incremental sheet forming. *J. Mater. Process. Technol.* **2009**, *209*, 3688–3695. [CrossRef]
2. Silva, M.B.; Skjødt, M.; Atkins, A.; Bay, N.; Martins, P.A.F. Single-point incremental forming and formability—Failure diagrams. *J. Strain. Anal. Eng.* **2008**, *43*, 15–35. [CrossRef]
3. Sebastiani, G. *Erweiterung der Prozessgrenzen inkrementeller Blechumformverfahren Mittels Flexibler Werkzeuge*; Shaker Verlag: Aachen, Germany, 2016; pp. 85–102.
4. Maqbool, F.; Bambach, M. Revealing the dominant forming mechanism of single point incremental forming (SPIF) by splitting plastic energy dissipation. *Procedia Eng.* **2017**, *183*, 188–193. [CrossRef]
5. Klocke, F.; König, W. *Fertigungsverfahren 4: Umformen*, 5rd ed.; Springer: Berlin/Heidelberg, Germany, 2006.
6. Bambach, M.; Ames, J.; Azaouzi, J.; Campagne, M.; Hirt, G.; Batoz, J. Initial experimental and numerical investigations into a class of new strategies for single point incremental forming (SPIF). In Proceedings of the 8th Int. ESAFORM Conference on Material Forming, Cluj-Napoca, Romania, 27–29 April 2005; pp. 671–674.
7. Hagan, E.; Jeswiet, J. A review of conventional and modern single-point sheet metal forming methods. *Proc. Inst. Mech. Eng. Part B J. Eng. Manuf.* **2003**, *217*, 213–225. [CrossRef]
8. Kim, T.; Yang, D. Improvement of formability for the incremental sheet metal forming process. *Int. J. Mech. Sci.* **2000**, *42*, 1271–1286. [CrossRef]

9. Tekkaya, A.E. Equivalent strain and stress history in torsion tests. *Steel Res. Int.* **1994**, *65*, 65–70. [CrossRef]
10. Emmens, W.C. *Formability—A Review of Parameters and Processes that Control, Limit or Enhance the Formability of Sheet Metal*; Springer: Berlin/Heidelberg, Germany, 2011.
11. Eyckens, P.; Moreau, J.; Duflou, J.; Van Bael, A.; Van Houtte, P. MK modelling of sheet formability in the incremental sheet forming process, taking into account through-thickness shear. *Int. J. Mater. Form.* **2009**, *2*, 379. [CrossRef]
12. Jackson, K.; Allwood, J. The mechanics of incremental sheet forming. *J. Mater. Process. Technol.* **2009**, *209*, 1158–1174. [CrossRef]
13. Martins, P.A.F.; Bay, N.; Skjødt, M.; Silva, M. Theory of single point incremental forming. *CIRP Ann.* **2008**, *57*, 247–252. [CrossRef]
14. Maaß, F.; Gies, S.; Dobecki, M.; Brömmelhoff, K.; Tekkaya, A.E.; Reimers, W. Analysis of residual stress state in sheet metal parts processed by single point incremental forming. In *AIP Conference Proceedings*; AIP Publishing: Melville, NY, USA, 2018; Volume 1960, p. 160017.
15. Lemaitre, J.; Chaboche, J.L. *Mechanics of Solid Materials*, 1st ed.; Cambridge University Press: Cambridge, UK, 1990; pp. 226–252.
16. Ambrogio, G.; Costantino, I.; De Napoli, L.; Filice, L.; Fratini, L.; Muzzupappa, M. On the influence of some relevant process parameters on the dimensional accuracy in Incremental Forming: A numerical and experimental investigation. *J. Mater Process. Technol.* **2003**, *153*, 501–507. [CrossRef]
17. Bhattacharya, A.; Maneesh, K.; Venkata, N.; Cao, J. Formability and surface finish studies in single point incremental forming. *J. Manuf. Sci. Eng.* **2011**, *133*, 621–627. [CrossRef]
18. Maaß, F.; Hahn, M.; Tekkaya, A.E.; Dobecki, M.; Poeche, A.; Brömmelhoff, K.; Reimers, W. Forming mechanisms-related residual stress development in single point incremental forming. *Prod. Eng.* **2019**, *13*, 149–156. [CrossRef]
19. Svensson, N. Anisotropy and the Bauschinger effect in cold rolled aluminum. *J. Mech. Eng. Sci.* **1966**, *8*, 162–172. [CrossRef]
20. Maaß, F.; Dobecki, M.; Hahn, M.; Reimers, W.; Tekkaya, A.E. Setting Component Properties in Incremental Forming. In Proceedings of the Contributed Papers from Materials Science and Technology, Portland, OR, USA, 29 September–3 October 2019; pp. 1176–1182. [CrossRef]